TGFβ1 Improves the Proliferation of Decellularized and Aligned Skeletal Muscle in Extracellular Matrix Hydrogels by m^{6}A Modification-Mediated Integrin Through Inducing ERK Phosphorylation

Menghai Zhu
The Third Affiliated Hospital of Southern Medical University https://orcid.org/0000-0002-1951-0815
Bengang Qin
Sun Yat-sen University First Affiliated Hospital
Yang Yi
Sun Yat-sen University First Affiliated Hospital
Jiantao Yang
Sun Yat-sen University First Affiliated Hospital
Liqiang Gu (✉ guliqiang1963@aliyun.com)
Sun Yat-sen University First Affiliated Hospital

Research Article

Keywords: N6-methyladenosine (m6A) RNA, skeletal muscle extracellular matrix hydrogel, skeletal muscle stem cells, TGFβ1.

Posted Date: July 16th, 2021

DOI: https://doi.org/10.21203/rs.3.rs-705252/v1

Abstract

Background: The purpose of this study was to illustrate the characteristics of skeletal muscle ECM hydrogels and assess the function and underlying mechanisms of hydrogels combined with TGFβ1 for the myogenesis of skeletal muscle stem cells (SkMSCs).

Methods: Six methods were used to obtain extracellular matrix (ECM) from rat skeletal muscle. Hydrogel components and cytocompatibility were assessed by Masson's trichrome staining, scanning electron microscopy, the sulfated glycosaminoglycan (s-GAG) and bFGF contents and a cell viability assay. Satellite cells were sorted, identified and seeded into skeletal muscle ECM hydrogels with TGFβ1. To determine the function of decellularized aligned skeletal muscle ECM hydrogels with TGFβ1 for the proliferation and differentiation of SkMSCs, a 3-(4,5-dimethylthiazol-2-yl)-2,5-diphenyltetrazolium bromide (MTT) assay, 5-ethynyl-2'-deoxyuridine (EdU) analysis and immunofluorescence staining were conducted. RNA stability assay and Gene set enrichment analysis (GSEA) were used to further investigated the mechanism underlying the function.

Results: Our study established a highly efficient method for the decellularization of skeletal muscle and fabricated an ECM hydrogel without cell components that preserves the rich ECM composition. This hydrogel formed a three-dimensional microstructure and showed good biocompatibility. We found that the decellularized aligned ECM scaffold with TGFβ1 promoted SkMSC proliferation and suppressed SkMSC differentiation through extracellular signal-regulated kinase (ERK) signaling. Our study suggested that TGFβ1 increases the m6A methylation of the integrin mRNA 3'UTR, thereby inducing the phosphorylation of ERK and promoting SkMSCs proliferation and differentiation.

Conclusions: Our study explored a highly efficient method for the decellularization of skeletal muscle and fabricated an ECM hydrogel with a three-dimensional microstructure and good biocompatibility. Furthermore, we demonstrated that decellularized aligned ECM scaffolds with TGFβ1 promoted SkMSC proliferation and differentiation through enhancing the m^6A methylation of the integrin mRNA 3'UTR, which may serve as a potential therapeutic strategy for the acute and chronic muscle injuries

Background

Severe trauma due to traffic accidents, severe injuries, and long-term denervation injury resulting in soft tissue loss is considered one of the most frequent clinical problems, and surgical reconstruction does not fully repair the tissue and frequently causes donor site morbidity[1–4]. Therefore, new treatment methods must be explored for severe skeletal muscle injuries[5–7].

Decellularized extracellular matrix (ECM) is a common material adopted for the rehabilitation and reconstruction of damaged tissues, and it can be obtained by various techniques involving physical methods, chemical reagents and/or biological reagents[6, 8, 9]. Various decellularized ECM-derived biomaterials, such as small intestine submucosa and urinary bladder tissue, have been adopted; however, these materials have limitations associated with heterogeneity [10–14]. Hydrogels made by ECM are

three-dimensional (3D) scaffolds that have a similar three-dimensional microstructure to that of native ECM[12, 15, 16]. A previous study focused on improving tissue regeneration and function after major trauma reported that an ECM hydrogel implanted in skeletal muscle has the potential to function in tissue development, structural support, and force transmission. However, the results are still not entirely satisfactory.

Many studies have reported that skeletal muscle stem cells (SkMSCs) can promote muscle regeneration and can be transplanted to damaged tissues[17–19]. In addition, substantial evidence suggests that TGF-β1 regulates the regeneration of muscle[20–22], and reports have indicated that C2C12 and SkMSCs can be activated via the extracellular signal-regulated kinase-1/2 (ERK1/2) pathway, which is involved in muscle cell proliferation and differentiation[19, 23]. To optimally utilize SkMSCs, we investigated the behavior of SkMSCs on synthetic skeletal muscle ECM hydrogels with TGF-β1 in vitro.

To identify the regulatory mechanisms of the ERK pathway, we found that it may be related to the N6-methyladenosine (m^6A) methylation modification. Some studies have reported the function of m^6A modification, such as mRNA stability, splicing, and translation[24, 25]. Recent studies demonstrated that METTL3 enhances cell adhesion by stabilizing integrin β1 in prostatic carcinoma[26]. In addition, studies have indicated that m^6A modification of integrin6 mRNA regulates the development and progression of bladder cancer[27]. Integrin 4 regulates airway epithelial cells through the EGFR, ERK and NF-κB pathways[28]. However, the mechanism of METTL3-mediates m^6A modification of integrin to regulate the proliferation and differentiation of SkMSCs has not been reported.

The purpose of this study was to explore and illustrate the characteristics of skeletal muscle ECM hydrogels and assess the function of hydrogels combined with TGFβ1 for the myogenesis of SkMSCs. We further proposed that TGF-β1 can regulate SkMSCs proliferation and differentiation through the METTL3/integrin/ ERK signaling axis.

Materials And Methods

Animals and cell culture

Fresh skeletal muscle was obtained from 8-week-old Sprague-Dawley rats. Rat tibialis muscles were dissociated by collagenase type I (0.2% collagenase, Sigma), then were filtered through a 40 μm filter (Biosharp). After isolation, myofiber-associated cells were subjected to flow cytometry analysis (see below). Markers for CD45 (BD Pharmingen), CD11b (BD Pharmingen), anti-integrinβ1 (ab95622, Abcam) and CD34 (ab81289, Abcam) were used. After sorting, cells were cultured in DMEM supplemented with 20% FBS and 1% chick embryo extract. Myogenic differentiation was induced using DMEM supplemented with 2% heat-inactivated horse serum.

Decellularization protocols

Fresh skeletal muscle (20 g) was obtained from 8-week-old adult Sprague-Dawley rats. Samples were decellularized at room temperature according to the following procedures: shaking in 1% SDS for 48 hours (method A), shaking in 0.2% sodium deoxycholate for 48 hours followed by shaking in 1% SDS for16 hours (method B), shaking in 1% Triton X-100 for 36 hours followed by shaking in 1% SDS for 36 hours (method C), shaking in 0.1% ethylenediaminetetraacetic acid (EDTA) for 6 hours followed by shaking in 0.2% sodium deoxycholate for 8 hours (method D), shaking in 0.2% trypsin/0.1% EDTA for 36 hours followed by shaking in 0.5% Triton X-100 at for 48 hours (method E), or shaking in 0.1% EDTA for 6 hours followed by shaking in 1% SDS for 12 hours (method F). Then, we removed the remaining nuclear materials by shaking in 9×106 U/l DNase-I (Thermo Fisher Scientific, USA) and 6×107 U/l RNase (Yami Biotechnology Co., Ltd., Beijing) for 24 hours. Finally, residual reagents were removed from the samples by repeated washes with deionized water and centrifugation.

Histological analysis

Samples were fixed in 4% paraformaldehyde for 24 hours and then processed according to the manufacturer's instructions. Staining with hematoxylin and eosin (H&E), Masson's trichrome and 4',6-diamidino-2-phenylindole (DAPI) (Vector Laboratories, Burlingame, CA, USA) was performed. Images of the samples were obtained using an Axio Observer Z1 inverted microscope (Carl Zeiss, Inc., Germany) with an Axiovision 4.8 camera.

Preparation of decellularized rat skeletal muscle matrix hydrogel and assessment of its properties

To prepare the decellularized skeletal muscle matrix hydrogel, 10 mg of ECM powder was put into 900 μl pepsin (Sigma-Aldrich) solution (0.01 M HCl, pepsin: ECM = 1:10) and then incubated under shaking for 48 hours until dissolved. After NaOH was added to stop the reaction. Then, phosphate-buffered saline (PBS) was added and evenly mixed and the mixture was incubated at 37°C for 30 min, 2 hours, and 24 hours for in vitro gelation. The matrix solution (500 μl) was placed at 37°C for gelation and assessed every 20 min. The ECM hydrogel was disinfected under ultraviolet light and its thickness was very thin.

Quantitative analysis of the DNA content, protein content and growth factors

The DNA content of fresh skeletal muscle, ECM and hydrogel was analyzed by a dsDNA Assay Kit (Invitrogen Inc.). To evaluate the protein content in the three kinds of samples, a bicinchoninic acid (BCA) protein detection kit (Sigma-Aldrich) was adopted. A Blyscan GAG Assay Kit (Biocolor) and rat enzyme-linked immunosorbent assays (ELISAs) (Minneapolis, MN) were used to quantitatively identify the levels of sulfated glycosaminoglycans (s-GAG) and fibroblast growth factor (bFGF).

Scanning electron microscopy

All samples were prepared according to the manufacturer's instructions prior to analysis via scanning electron microscopy. Sample cross-sections were analyzed by a scanning electron microscope (Quanta 250, FEI) at an accelerating voltage of 30 kV.

Flow cytometry

Flow cytometry analysis and cell sorting were performed at the central laboratory of The First Affiliated Hospital of Sun Yat-sen University. Both sorting and analysis were carefully performed according to the manufacturer's instructions.

Quantitative real-time polymerase chain reaction (qRT-PCR)

Total RNA extraction and amplification were performed according to the manufacturer's instructions. The following primers were used: Pax7: forward 5'-AGCCGAGTGCTCAGAATCAA-3' and reverse 5'-TCCTCTCGAAAGCCTTCTCC-3', MyoD: forward 5'CGACTGCCTGTCCAGCATAG-3' and reverse 5'-GGACACTGAGGGGTGGAGTC-3', MyHC: forward 5'-TGCCAAGACCGTGAGGAATG-3' and reverse 5'-AATGCATCACAGCTCCCGTG-3', and GAPDH: forward 5'-GGGTGATGCTGGTGCTGAGTATGT-3' and reverse 5'-AAGAATGGGAGTTGCTGTTGAAGTC-3'.

Cell viability analysis

MTT assay was performed according to the manufacturer's instructions. SkMSCs were seeded in 96-well plates (1 × 104 cells/ml) coated with or without decellularized skeletal muscle ECM hydrogels. The concentration of solubilized MTT formazan was measured by a microplate reader (TECAN, Austria) at an absorbance wavelength of 490 nm.

Cell proliferation assay

A 5-ethynyl-2'-deoxyuridine (EdU) kit (RiboBio, Guangzhou) was adopted to evaluate the proliferation of SkMSCs. Briefly, SkMSCs were seeded in 6-well plates (8×105 cells/well) coated with decellularized skeletal muscle ECM hydrogels and cultured in growth medium and then sorted into the following four treatment groups: NC group, TGFβ1 group (2.5 ng/ml TGFβ1), TGFβ1 + PD98059 group (2.5 ng/ml TGFβ1 + 10 μM PD9809) and PMA group (25 nmol/L phorbol 12-myristate 13-acetate (PMA).

Immunofluorescence staining and microscopy

Cultures were fixed with 4% paraformaldehyde, processed for single and double

immunofluorescence and stained with DAPI to identify the nuclei. Primary antibodies against PAX7 (1:100 dilution, ab199010, Abcam, USA), MyoD (1:250 dilution, ab203383, Abcam), myosin heavy chain (1:200 dilution, ab11083, Abcam, USA), anti-laminin (ab11575), anti-collagen IV (ab6586), and anti-desmin [Y66] cytoskeletal markers (ab32362) (1:100 dilution, ab129002, Abcam, Cambridge, MA, USA) were used. Matching secondary antibodies conjugated to goat anti-mouse IgG H&L (1:1000 dilution, Alexa Fluor® 594) (ab150116) and goat anti-rabbit IgG H&L (Alexa Fluor® 488) (1:1000 dilution, ab150077, Abcam) were used. Cell nuclei were counterstained with DAPI (ab228549, Abcam, USA). Cell images were obtained by an Axiovision 4.8 camera and an Axio Observer Z1 inverted microscope (Carl Zeiss, Inc., Germany).

Confocal electron microscopy

Cells were seeded on confocal dishes and maintained in an incubator for 24 hour. The procedures were performed according to the manufacturer's instructions. The primary antibodies included Pax7 (1:200 dilution) and MyoD (1:200 dilution), which were then incubated with goat anti-mouse IgG H&L (1:1000 dilution, Alexa Fluor® 594) (ab150116) and goat anti-rabbit IgG H&L (Alexa Fluor® 488) (1:1000 dilution, ab150077, Abcam) for 1 hour in the dark at room temperature. Then, DAPI was added and a confocal microscope (Nikon) was used to acquire images.

Dual-luciferase reporter assay

The luciferase reporter assay was performed using the Dual-Luciferase Reporter Assay System (Promega). Cells were transfected with pmiGLO-based luciferase vector fused or not fused to the wild-type or mutated integrin–3'UTR. METTL3 or empty vectors were cotransfected.

RNA stability assay

Actinomycin D (Sigma-Aldrich) was added to SkMSCs at 5 mg/ml to assess RNA stability. After incubation for indicated time points, the cells were collected and RNA samples were extracted for reverse transcription and qPCR. mRNA transcription was inhibited with Actinomycin D and the degradation rate of RNA (K decay) was estimated.

Statistical analysis

Statistically significant differences were determined by t-tests for comparisons between two groups and by one-way analysis of variance (ANOVA) for comparisons between more than two groups. All data were analyzed using SPSS 22.0 software.

Results

Preliminary evaluation of decellularized skeletal muscle ECM

Decellularization can be performed according to six methods (A-F). H&E and DAPI staining (Fig. 1A) did not identify intact nuclei on the decellularized skeletal muscle ECM compared with that on fresh muscle. The residual content of DNA after decellularization was quantified as shown in Fig. 1B. The protein content of the decellularized ECM from rat muscle tissue is shown in Fig. 1C. The acellular matrix and fresh muscle results showed that the protein laminin and type IV collagen were expressed, and immunofluorescence showed that the location was on the basement membrane. Significant differences were not observed among the different groups (Fig. 1D).

Evaluation of decellularized skeletal muscle ECM hydrogels.

Masson's trichrome staining was used to assess the properties of the decellularized skeletal muscle ECM hydrogels (Fig. 2A). Masson's trichrome staining of the fresh muscle, decellularized ECM and hydrogel

indicated changes in the properties. In all samples, collagen was located in the stromal compartment of the tissues, although significant differences were not observed among the three groups. Scanning electron microscopy (SEM) revealed that skeletal muscle consisted of many muscle fibers while the hydrogel consisted of a porous structure with various pore sizes (Fig. 2B). The content of GAG is shown in Fig. 2C. In the skeletal muscle ECM and fresh muscle, 0.66 ± 0.09 μg/mg and 3.09 ± 0.32 μg/mg of s-GAG were observed, respectively, whereas in the hydrogel, this amount was only 0.64 ± 0.08 μg/mg.

A BCA protein assay was performed for the remaining proteins in the skeletal muscle ECM, hydrogel, and fresh muscle (Fig. 2D). The amounts of protein from the skeletal muscle ECM and hydrogel were 0.23 ± 0.09 and 0.19 ± 0.07 mg protein/g dry weight, respectively, which were two orders of magnitude less than the amount extracted from fresh muscle (0.46 ± 0.12 μg/mg tissue). The total amounts of bFGF are shown in Fig. 2E. The hydrogel retained bFGF, whereas lower amounts of bFGF were retained in the hydrogel than the skeletal muscle ECM. The total bFGF content was 8.9 ± 1.8 ng bFGF/g dry weight in the hydrogel, which was less than that in the skeletal muscle ECM (9.5 ± 2.3 ng bFGF/g dry weight) and fresh muscle (20.2 ± 4.6 ng bFGF/g dry weight). As shown in Fig. 2F, the bFGF values normalized to the amount of total extracted protein were similar for the skeletal muscle ECM, hydrogel, and fresh muscle (5.9 ± 2.4, 5.78 ± 1.8, and 1.8 ± 0.21 ng bFGF/mg protein, respectively). To further confirm cell viability, stem cells seeded on the hydrogel scaffolds or seeded in empty wells (NC) were analyzed by an MTT assay (Fig. 2G), and significant differences were not observed between the two groups.

Isolation and identification of SkMSCs

FACS analysis suggested that SkMSCs were positive for CD34 and integrin β1 and negative for CD11b and CD45 (Fig. 3C). SkMSCs were confirmed via light microscopy to have a fibroblast-like morphology. To investigate the characteristics of SkMSCs, we examined the expression of Pax7 and MyoD. As shown in Fig. 3B, the majority of adhered SkMSCs showed robust expression of Pax7 and MyoD. After culture in DMEM supplemented with 2% heat-inactivated horse serum, the cells showed more robust expression of MyoD over time while Pax7 showed the opposite expression pattern (Fig. 3C and D). Furthermore, we analyzed the expression of Pax7, MyoD, desmin and MyHC in undifferentiated and differentiated cells. Consistent with these data, the percentage of Pax7-positive cells was significantly lower among differentiated cells than among undifferentiated cells. Compared with the Pax7 expression pattern, the percentage of MyoD-, desmin- and MyHC-positive cells markedly increased over time (Fig. 3E).

Aligning ECM hydrogels with TGFβ1 affected the proliferation and differentiation of SkMSCs

Initially, we investigated the effect of ECM hydrogels with TGFβ on the survival of SkMSCs using an MTT assay. The results showed that hydrogels combined with TGFβ1 significantly promoted cell viability compared with the control group (Fig. 4A). Moreover, significant differences were not observed in cell viability between the NC and hydrogel groups. Furthermore, immunofluorescence staining suggested that the expression of MyoD and MyHC was the lowest in the hydrogel + TGFβ1 group (Fig. 4B, C). Finally, significantly downregulated expression of MyoD and MyHC was observed in the hydrogel + TGFβ1 group,

which was further confirmed by western blot analysis (Fig. 4D, E). These data revealed that ECM hydrogels aligned with TGFβ1 promoted SkMSC proliferation and inhibited SkMSC differentiation.

ECM hydrogels aligned with TGFβ1 regulated the proliferation and differentiation of SkMSCs through ERK signaling

To further investigate the mechanism underlying the function of the aligned ECM hydrogels with TGFβ1 in terms of the proliferation and differentiation of SkMSCs, EdU assays were performed (Fig. 5A, B), and they demonstrated that TGFβ1 promoted SkMSC proliferation. An inhibitor of ERK signaling (PD98059) reversed this trend, while an activator of ERK signaling (PMA) enhanced cell proliferation. Immunofluorescence staining showed that TGFβ1 significantly attenuated the expression of MyoD and MYHC (Fig. 5C, D). Moreover, the expression of MyoD and MyHC was upregulated by PD98059 and downregulated by PMA due to the inhibition or enhancement of ERK signaling, respectively. Consistent with these data, the qRT-PCR (Fig. 5E) and western blot assays (Fig. 5F, G) showed that TGFβ1 suppressed ERK signaling, MyoD expression and MYHC expression, PD98059 reversed the TGFβ1 function, and p-ERK showed the opposite trend. Therefore, these results indicated that the ECM hydrogels aligned with TGFβ1 regulated the proliferation and differentiation of SkMSCs through ERK signaling.

m^6A modification-mediated integrin regulates the proliferation and differentiation of SkMSCs through inducing ERK signaling

To investigate the mechanism by which TGFβ1 regulates the proliferation and differentiation of SkMSCs through ERK signaling, q-PCR was performed, revealing that TGFβ1 promoted METTL3 and integrin expression, while inhibition of TGFβ1 reduced the levels of METTL3 and integrin (Fig. 6A). Consistent with these data, western blot analysis suggested that TGFβ1 increased METTL3 and integrin expression, while inhibition of TGFβ1 suppressed their expression (Fig. 6B, C). Then METTL3-KO decreased the expression of integrin, but METTL3 overexpression enhanced integrin expression. Furthermore, to determine whether TGFβ1 is a direct target of METTL3, we performed luciferase reporter assays. The luciferase activity of SkMSCs-METTL3-KO transfected with a reporter construct carrying wild-type integrin 3’ UTR and CDS was decreased compared with that of METTL3-OE SkMSCs, this decrease was abrogated in mutated SkMSCs (Fig. 6D). As expected, forced expression of wild-type METTL3 increased the m^6A levels of integrin mRNA and enhanced the luciferase activity of the reporter construct carrying the wild-type integrin 3’ UTR and CDS relative to that of the control (Fig. 6E). To explore the biological function of METTL3-mediated m^6A modification in integrin mRNA metabolism, actinomycin D (Sigma-Aldrich) was added to SkMSCs to assess RNA stability. Knockdown of METTL3 decreased, while METTL3 overexpression improved, the mRNA stability of integrin (Fig. 6F, G). The results showed that METTL3 knockdown induced the downregulation of integrin in SkMSCs, suggesting that METTL3 regulates integrin synthesis by modulating the stability and/or translation of integrin mRNA. Taken together, our results demonstrated that the modulation of integrin expression was under the control of METTL3-associated m^6A modification.

We next identify the mechanism by which integrin regulates SkMSC proliferation and differentiation. Gene set enrichment analysis (GSEA) demonstrated that integrin was related to the MAPK signaling pathway (Fig. 7A). Then, integrin downregulation greatly decreased ERK phosphorylation (Fig. 7B), while upregulation of integrin enhanced ERK phosphorylation (Fig. 7C). Then, western blot assays also showed the levels of p-ERK when integrin was upregulated (Fig. 7D, E). Moreover, the effect of p-ERK on integrin in SkMSCs was examined using PMD98089 (an ERK-specific inhibitor) and it suggested that PMD98089 reduced the inhibitory effect on ERK phosphorylation of integrin. Furthermore, downregulation of p-ERK in SkMSCs by integrin knockdown abrogated the increased proliferation (Fig. 7G). Moreover, qPCR showed that integrin promoted the mRNA expression of Pax7, MyoD and MyHC, indicating proliferation, while PMD98089 abolished the enhancing effect of integrin (Fig. 7H). Western blot analysis also verified that the ERK-specific inhibitor reduced the promotional effect of integrin (Fig. 7I). These data suggest that m^6A modification-mediated changes in ERK signaling path may be the mechanism underlying of integrin in SkMSCs.

Discussion

Injuries to extremities due to traffic accidents and prolonged denervation result in soft tissue loss and are considered the most frequent clinical problem[1, 2, 4]. In recent years, stem cell transplantation therapy has been considered an effective strategy for the regeneration of damaged tissues. However, the therapeutic efficacy has been impeded by the poor viability of SkMSCs in injured tissues [11, 29]. To resolve the poor survival of transplanted cells, studies have been performed to promote the proliferation of SkMSCs. Our study explored a rapid method for skeletal muscle decellularization and fabricated an ECM hydrogel with a three-dimensional microstructure and good biocompatibility. Furthermore, we demonstrated that decellularized aligned ECM scaffolds with TGFβ1 promote SkMSC proliferation and SkMSC differentiation through ERK signaling.

Previous studies have demonstrated that decellularized ECM provides a structure to repair and reconstruct damaged tissues[14, 30, 31]. Recent studies have reported various methods for the decellularization of muscle tissue[8, 32].However, an insufficient treatment may cause inflammation and immune rejection because of the remaining antigenic cellular proteins. Furthermore, excessive decellularization, which could ensure biological safety, may damage the composition and structure of the ECM[14, 33, 34].In the present study, we evaluated decellularized skeletal muscle ECM hydrogels. The contents of GAG, bFGF, total protein and residual DNA were quantified in the different samples and found to be similar to the contents reported in previous studies on pig, mouse and rat hydrogels[8, 10, 13, 35]. To further confirm cell viability, SkMSCs were seeded on the hydrogel scaffolds and empty wells (NC) and analyzed by an MTT assay, and significant differences were not observed between these two groups. Moreover, studies have suggested that hydrogels support cell growth and enhance myogenic protein expression[10, 36].

Stem cells are located in a majority of adult tissues and can be activated by acute and chronic injuries to exert a critical role in tissue growth and regeneration[37, 38]. Many studies have reported that cell sorting

by a series of cell surface markers that are characteristic of muscle stem cells can be used to prospectively identify skeletal muscle satellite cells[37–39]. We isolated particular cells by FACS and analyzed the expression of Pax7 and MyoD. To further investigate this hypothesis, we analyzed the expression of Pax7, MyoD, desmin and MYHC in undifferentiated and differentiated cells. Consistent with these data, the percentage of PAX7-positive cells was significantly lower among the differentiated cells than among the undifferentiated cells. Compared with the PAX7 expression pattern, the percentage of MyoD-, desmin- and MYHC-positive cells markedly increased over time.

Previous studies have shown that a prerequisite step in myogenic differentiation of SkMSCs is the activation of MyoD[18, 22, 40, 41]. Moreover, TGFβ1 was reported to regulate the ERK signaling pathway involved in inflammation, regeneration and differentiation[42, 43]. To further investigate the mechanism underlying the function of the ECM hydrogels aligned with TGFβ1 in terms of the proliferation and differentiation of SkMSCs, the EdU assays demonstrated that TGFβ1 promoted SkMSC proliferation. An inhibitor of ERK signaling reversed this trend, while an activator of ERK signaling enhanced cell proliferation. Immunofluorescence staining was performed and showed that TGFβ1 significantly attenuated the expression of MyoD and MYHC. Our results indicated that the ECM hydrogels aligned with TGFβ1 regulated the proliferation and differentiation of SkMSCs through ERK signaling. To identify the regulatory mechanisms of the ERK pathway, we found that it was related to m^6A modification.

Integrin activates FAK/paxillin/AKT signaling pathway and affects the expression of the proliferative marker Ki67 in tumors[44]. Recent studies have shown that transmembrane integrin α2β1 directly interacts with lumican, and activates ERK and ALP activities in osteoblasts[45]. Our study first indicated that METTL3 regulates integrin and attenuates its m^6A-mediated degradation. Here, we proved that METTL3 enhanced integrin. which therefore promoted ERK phosphorylation in SkMSCs. However, whether METTL3 induces mRNA alternative splicing or affects the mRNA stability of integrin remains to be further studied. Our further studies will focus on the exact binding site of integrin that interacts with ERK signaling and the molecular mechanism by which integrin activates ERK signaling in SkMSCs.

Conclusion

In summary, our study imply that decellularized ECM scaffolds aligned with TGFβ1 promote SkMSC proliferation and SkMSC differentiation through ERK signaling by m^6A-mediated integrin. Furthermore, upregulation of integrin is related the substantial ability of SkMSCs to proliferate and differentiate. Thus, integrin might be a promising therapeutic target for the regeneration of damaged tissues.

Abbreviations

ECM, decellularized extracellular matrix; MyHC, myosin heavy chain; Myod, myogenic differentiation markers; m^6A, N6-methyladenosine RNA; Pax7, paired box (Pax) protein7; SkMSCs, skeletal muscle stem cells; TGFβ1, transforming growth factor-beta1.

Declarations

Authors' contributions: Menghai Zhu carried out experiments, data analysis, and wrote the manuscript. Bengang Qin and Yi Yang performed experiments and helped with data quantifications. Liqiang Gu, Jiantao Yang designed the project, supervised the experiment.

Funding: This work was supported by the National Natural Science Foundation Item (81871787 and 81601057), Natural Science Foundation of Guangdong Province (2018A030310254 and 2015A030310350). Research Fund of Medical Science and Technology in Guangdong Province A2017190and Youth Start-Up Fund(grant nos. QN2020005).

Data Availability Statement

The data used to support the findings of this study are included within the article.

Ethics statement

Animal care was approved by the Institutional Animal Care and Use Committee at The First Affiliated Hospital of Sun Yat-sen University. All experimental procedures and methods were performed according to the relevant guidelines and regulations.

Consent for publication Not applicable.

Acknowledgements: Not applicable.

Declaration of interest

The authors declare no conflicts of interest.

References

1. A. Meyer, K. Goller, R.E. Horch, J.P. Beier, C.D. Taeger, A. Arkudas, W. Lang, Results of combined vascular reconstruction and free flap transfer for limb salvage in patients with critical limb ischemia, Journal of vascular surgery, 61 (2015) 1239-1248.
2. M. Barla, B. Gavanier, M. Mangin, J. Parot, C. Bauer, D. Mainard, Is amputation a viable treatment option in lower extremity trauma?, Orthopaedics & traumatology, surgery & research : OTSR, 103 (2017) 971-975.
3. T. Garbenyte-Apolinskiene, S. Salatkaite, L. Siupsinskas, R. Gudas, Prevalence of Musculoskeletal Injuries, Pain, and Illnesses in Elite Female Basketball Players, Medicina, 55 (2019).
4. K.J. Agarwal-Harding, L.C. Chokotho, N.C. Mkandawire, C. Martin, Jr., E. Losina, J.N. Katz, Risk Factors for Delayed Presentation Among Patients with Musculoskeletal Injuries in Malawi, The Journal of bone and joint surgery. American volume, 101 (2019) 920-931.

5. W. Liang, B.K. Tan, Use of the cross-leg distally based sural artery flap for the reconstruction of complex lower extremity defects, Archives of plastic surgery, 46 (2019) 255-261.
6. B.J. Kwee, D.J. Mooney, Biomaterials for skeletal muscle tissue engineering, Current opinion in biotechnology, 47 (2017) 16-22.
7. C.A. Cezar, D.J. Mooney, Biomaterial-based delivery for skeletal muscle repair, Advanced drug delivery reviews, 84 (2015) 188-197.
8. Y. Fu, X. Fan, C. Tian, J. Luo, Y. Zhang, L. Deng, T. Qin, Q. Lv, Decellularization of porcine skeletal muscle extracellular matrix for the formulation of a matrix hydrogel: a preliminary study, Journal of cellular and molecular medicine, 20 (2016) 740-749.
9. M. Piccoli, C. Trevisan, E. Maghin, C. Franzin, M. Pozzobon, Mouse Skeletal Muscle Decellularization, Methods in molecular biology, 1577 (2018) 87-93.
10. S.A. Hurd, N.M. Bhatti, A.M. Walker, B.M. Kasukonis, J.C. Wolchok, Development of a biological scaffold engineered using the extracellular matrix secreted by skeletal muscle cells, Biomaterials, 49 (2015) 9-17.
11. B.T. Ledford, J. Simmons, M. Chen, H. Fan, C. Barron, Z. Liu, M. Van Dyke, J.Q. He, Keratose Hydrogels Promote Vascular Smooth Muscle Differentiation from C-kit-Positive Human Cardiac Stem Cells, Stem cells and development, 26 (2017) 888-900.
12. J.A. Passipieri, H.B. Baker, M. Siriwardane, M.D. Ellenburg, M. Vadhavkar, J.M. Saul, S. Tomblyn, L. Burnett, G.J. Christ, Keratin Hydrogel Enhances In Vivo Skeletal Muscle Function in a Rat Model of Volumetric Muscle Loss, Tissue engineering. Part A, 23 (2017) 556-571.
13. J. Radhakrishnan, U.M. Krishnan, S. Sethuraman, Hydrogel based injectable scaffolds for cardiac tissue regeneration, Biotechnology advances, 32 (2014) 449-461.
14. J.M. Singelyn, P. Sundaramurthy, T.D. Johnson, P.J. Schup-Magoffin, D.P. Hu, D.M. Faulk, J. Wang, K.M. Mayle, K. Bartels, M. Salvatore, A.M. Kinsey, A.N. Demaria, N. Dib, K.L. Christman, Catheter-deliverable hydrogel derived from decellularized ventricular extracellular matrix increases endogenous cardiomyocytes and preserves cardiac function post-myocardial infarction, Journal of the American College of Cardiology, 59 (2012) 751-763.
15. L.T. Saldin, M.C. Cramer, S.S. Velankar, L.J. White, S.F. Badylak, Extracellular matrix hydrogels from decellularized tissues: Structure and function, Acta biomaterialia, 49 (2017) 1-15.
16. Y.J. Choi, Y.J. Jun, D.Y. Kim, H.G. Yi, S.H. Chae, J. Kang, J. Lee, G. Gao, J.S. Kong, J. Jang, W.K. Chung, J.W. Rhie, D.W. Cho, A 3D cell printed muscle construct with tissue-derived bioink for the treatment of volumetric muscle loss, Biomaterials, 206 (2019) 160-169.
17. V. Chaturvedi, D.E. Dye, B.F. Kinnear, T.H. van Kuppevelt, M.D. Grounds, D.R. Coombe, Interactions between Skeletal Muscle Myoblasts and their Extracellular Matrix Revealed by a Serum Free Culture System, PloS one, 10 (2015) e0127675.
18. F. Chen, J. Zhou, Y. Li, Y. Zhao, J. Yuan, Y. Cao, L. Wang, Z. Zhang, B. Zhang, C.C. Wang, T.H. Cheung, Z. Wu, C.C. Wong, H. Sun, H. Wang, YY1 regulates skeletal muscle regeneration through controlling metabolic reprogramming of satellite cells, The EMBO journal, 38 (2019).

19. Y. Ohno, K. Ando, T. Ito, Y. Suda, Y. Matsui, A. Oyama, H. Kaneko, S. Yokoyama, T. Egawa, K. Goto, Lactate Stimulates a Potential for Hypertrophy and Regeneration of Mouse Skeletal Muscle, Nutrients, 11 (2019).
20. S.F. Badylak, J.L. Dziki, B.M. Sicari, F. Ambrosio, M.L. Boninger, Mechanisms by which acellular biologic scaffolds promote functional skeletal muscle restoration, Biomaterials, 103 (2016) 128-136.
21. K. Delaney, P. Kasprzycka, M.A. Ciemerych, M. Zimowska, The role of TGF-beta1 during skeletal muscle regeneration, Cell biology international, 41 (2017) 706-715.
22. S. Han, C. Cui, Y. Wang, H. He, Z. Liu, X. Shen, Y. Chen, D. Li, Q. Zhu, H. Yin, Knockdown of CSRP3 inhibits differentiation of chicken satellite cells by promoting TGF-beta/Smad3 signaling, Gene, 707 (2019) 36-43.
23. C.G. Buitrago, A.C. Ronda, A.R. de Boland, R. Boland, MAP kinases p38 and JNK are activated by the steroid hormone 1alpha,25(OH)2-vitamin D3 in the C2C12 muscle cell line, Journal of cellular biochemistry, 97 (2006) 698-708.
24. R. Kumari, P. Ranjan, Z.G. Suleiman, S.K. Goswami, J. Li, R. Prasad, S.K. Verma, mRNA modifications in cardiovascular biology and disease: with a focus on m6A modification, Cardiovascular research, (2021).
25. M. Mendel, K. Delaney, R.R. Pandey, K.M. Chen, J.M. Wenda, C.B. Vagbo, F.A. Steiner, D. Homolka, R.S. Pillai, Splice site m(6)A methylation prevents binding of U2AF35 to inhibit RNA splicing, Cell, (2021).
26. E. Li, B. Wei, X. Wang, R. Kang, METTL3 enhances cell adhesion through stabilizing integrin beta1 mRNA via an m6A-HuR-dependent mechanism in prostatic carcinoma, American journal of cancer research, 10 (2020) 1012-1025.
27. H. Jin, X. Ying, B. Que, X. Wang, Y. Chao, H. Zhang, Z. Yuan, D. Qi, S. Lin, W. Min, M. Yang, W. Ji, N(6)-methyladenosine modification of ITGA6 mRNA promotes the development and progression of bladder cancer, EBioMedicine, 47 (2019) 195-207.
28. L. Yuan, X. Zhang, M. Yang, X. Du, L. Wang, S. Wu, M. Wu, Z. Duan, G. Xiao, Y. Zou, Y. Xiang, X. Qu, H. Liu, L. Qin, Q. Qin, X. Qin, C. Liu, Airway epithelial integrin beta4 suppresses allergic inflammation by decreasing CCL17 production, Clinical science, 134 (2020) 1735-1749.
29. K. Yamashita, E. Inagaki, S. Hatou, K. Higa, A. Ogawa, H. Miyashita, K. Tsubota, S. Shimmura, Corneal Endothelial Regeneration Using Mesenchymal Stem Cells Derived from Human Umbilical Cord, Stem cells and development, 27 (2018) 1097-1108.
30. J. Zhang, Z.Q. Hu, N.J. Turner, S.F. Teng, W.Y. Cheng, H.Y. Zhou, L. Zhang, H.W. Hu, Q. Wang, S.F. Badylak, Perfusion-decellularized skeletal muscle as a three-dimensional scaffold with a vascular network template, Biomaterials, 89 (2016) 114-126.
31. B.M. Sicari, J.P. Rubin, C.L. Dearth, M.T. Wolf, F. Ambrosio, M. Boninger, N.J. Turner, D.J. Weber, T.W. Simpson, A. Wyse, E.H. Brown, J.L. Dziki, L.E. Fisher, S. Brown, S.F. Badylak, An acellular biologic scaffold promotes skeletal muscle formation in mice and humans with volumetric muscle loss, Science translational medicine, 6 (2014) 234ra258.

32. A. Urciuolo, L. Urbani, S. Perin, P. Maghsoudlou, F. Scottoni, A. Gjinovci, H. Collins-Hooper, S. Loukogeorgakis, A. Tyraskis, S. Torelli, E. Germinario, M.E.A. Fallas, C. Julia-Vilella, S. Eaton, B. Blaauw, K. Patel, P. De Coppi, Decellularised skeletal muscles allow functional muscle regeneration by promoting host cell migration, Scientific reports, 8 (2018) 8398.
33. M.T. Wolf, C.L. Dearth, S.B. Sonnenberg, E.G. Loboa, S.F. Badylak, Naturally derived and synthetic scaffolds for skeletal muscle reconstruction, Advanced drug delivery reviews, 84 (2015) 208-221.
34. Y. Efraim, H. Sarig, N. Cohen Anavy, U. Sarig, E. de Berardinis, S.Y. Chaw, M. Krishnamoorthi, J. Kalifa, H. Bogireddi, T.V. Duc, T. Kofidis, L. Baruch, F.Y.C. Boey, S.S. Venkatraman, M. Machluf, Biohybrid cardiac ECM-based hydrogels improve long term cardiac function post myocardial infarction, Acta biomaterialia, 50 (2017) 220-233.
35. A. Porzionato, M.M. Sfriso, A. Pontini, V. Macchi, L. Petrelli, P.G. Pavan, A.N. Natali, F. Bassetto, V. Vindigni, R. De Caro, Decellularized Human Skeletal Muscle as Biologic Scaffold for Reconstructive Surgery, International journal of molecular sciences, 16 (2015) 14808-14831.
36. K.H. Patel, A.J. Dunn, M. Talovic, G.J. Haas, M. Marcinczyk, H. Elmashhady, E.G. Kalaf, S.A. Sell, K. Garg, Aligned nanofibers of decellularized muscle ECM support myogenic activity in primary satellite cells in vitro, Biomedical materials, 14 (2019) 035010.
37. A. Sacco, R. Doyonnas, P. Kraft, S. Vitorovic, H.M. Blau, Self-renewal and expansion of single transplanted muscle stem cells, Nature, 456 (2008) 502-506.
38. K.K. Tanaka, J.K. Hall, A.A. Troy, D.D. Cornelison, S.M. Majka, B.B. Olwin, Syndecan-4-expressing muscle progenitor cells in the SP engraft as satellite cells during muscle regeneration, Cell stem cell, 4 (2009) 217-225.
39. M. Cerletti, S. Jurga, C.A. Witczak, M.F. Hirshman, J.L. Shadrach, L.J. Goodyear, A.J. Wagers, Highly efficient, functional engraftment of skeletal muscle stem cells in dystrophic muscles, Cell, 134 (2008) 37-47.
40. P. D'Andrea, M. Sciancalepore, K. Veltruska, P. Lorenzon, A. Bandiera, Epidermal Growth Factor - based adhesion substrates elicit myoblast scattering, proliferation, differentiation and promote satellite cell myogenic activation, Biochimica et biophysica acta. Molecular cell research, 1866 (2019) 504-517.
41. J.P. Sah, N.T.T. Hao, Y. Kim, T. Eigler, E. Tzahor, S.H. Kim, Y. Hwang, J.K. Yoon, MBP-FGF2-Immobilized Matrix Maintains Self-Renewal and Myogenic Differentiation Potential of Skeletal Muscle Stem Cells, International journal of stem cells, (2019).
42. X. Liu, S. Gao, H. Xu, lncRNAPCAT29 inhibits pulmonary fibrosis via the TGFbeta1regulated RASAL1/ERK1/2 signal pathway, Molecular medicine reports, 17 (2018) 7781-7788.
43. Y. Xu, H. Xiao, H. Luo, Y. Chen, Y. Zhang, L. Tao, Y. Jiang, Y. Chen, X. Shen, Inhibitory effects of oxymatrine on TGFbeta1induced proliferation and abnormal differentiation in rat cardiac fibroblasts via the p38MAPK and ERK1/2 signaling pathways, Molecular medicine reports, 16 (2017) 5354-5362.

44. Q. Yu, W. Xiao, S. Sun, A. Sohrabi, J. Liang, S.K. Seidlits, Extracellular Matrix Proteins Confer Cell Adhesion-Mediated Drug Resistance Through Integrin alpha v in Glioblastoma Cells, Frontiers in cell and developmental biology, 9 (2021) 616580.
45. J.Y. Lee, S.J. Park, D.A. Kim, S.H. Lee, J.M. Koh, B.J. Kim, Muscle-Derived Lumican Stimulates Bone Formation via Integrin alpha2beta1 and the Downstream ERK Signal, Frontiers in cell and developmental biology, 8 (2020) 565826.

Figures

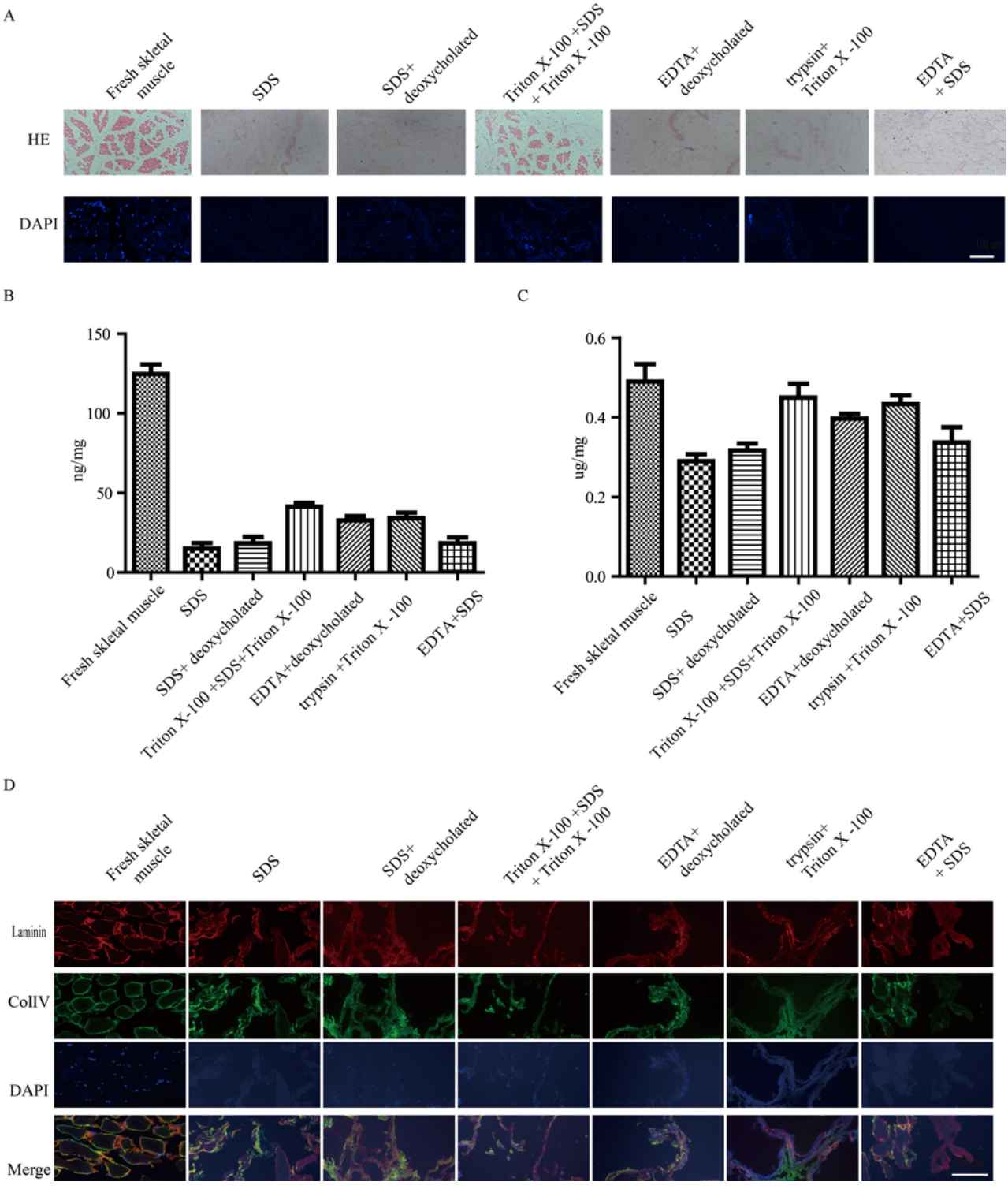

Figure 1

Evaluation of decellularized skeletal muscle ECM. (A) H&E staining and DAPI staining of rat skeletal muscle before and after decellularization with methods A-F. (B) DNA content in skeletal muscle and decellularized ECM obtained by methods A-F and determined by a Quant-iTTM PicoGreen dsDNA Assay Kit. (C) Protein content in skeletal muscle and decellularized ECM obtained by methods A-F and analyzed

using a BCA Assay Kit. (D) Immunofluorescence staining images of the expression of the myogenic markers laminin and collagen IV.

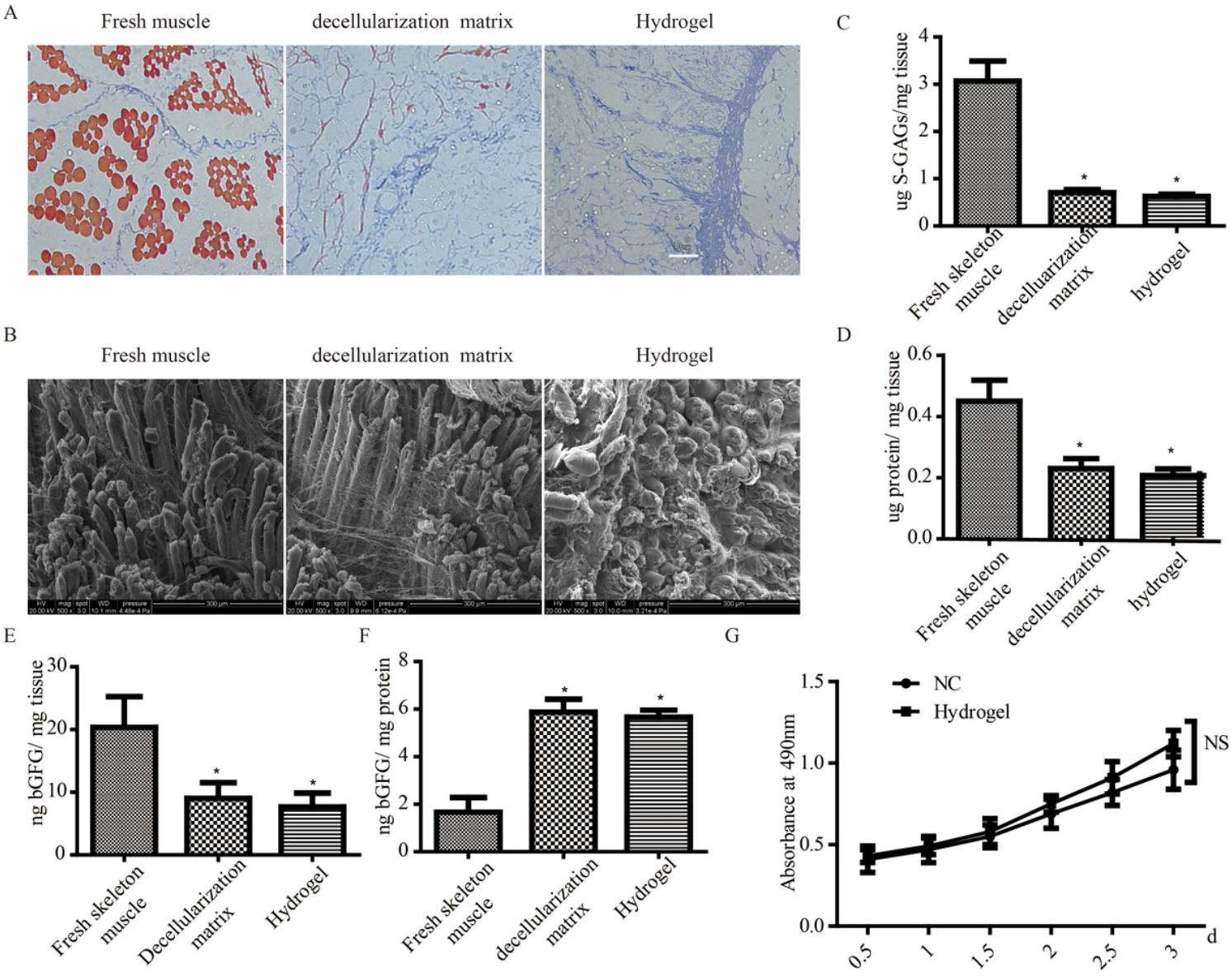

Figure 2

Evaluation of decellularized skeletal muscle ECM hydrogels. (A) Fresh skeletal muscle, decellularized skeletal muscle ECM and hydrogel were stained with Masson's trichrome. (B) Scanning electron microscopy of cross-sections of fresh skeletal muscle tissue, decellularized skeletal muscle ECM and hydrogel. (C) Quantification of the s-GAG content in fresh skeletal muscle tissue, decellularized skeletal muscle ECM and hydrogel. (D) Quantification of proteins in fresh skeletal muscle tissue, decellularized skeletal muscle ECM and hydrogel. (E) Quantification of bFGF in fresh skeletal muscle tissue, decellularized skeletal muscle ECM and hydrogel. (F) Quantification of bFGF normalized to the protein content in fresh skeletal muscle tissue, decellularized skeletal muscle ECM and hydrogel. Panel (C) shows the total extracted bFGF per initial dry weight of tissue, and panel (D) shows the total extracted bFGF normalized to the total soluble extracted protein. (G) Cell viability was determined by an MTT assay.

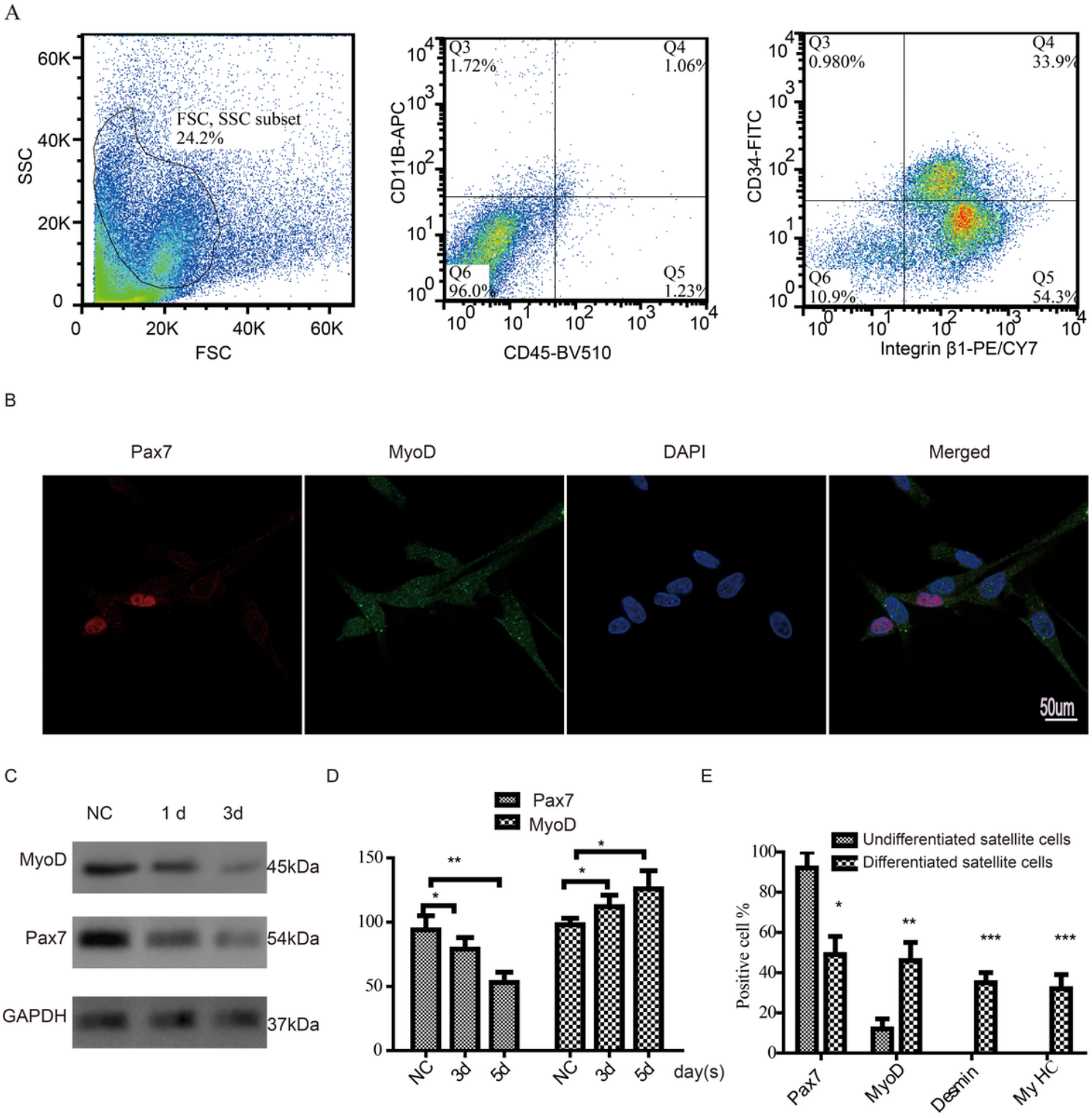

Figure 3

Isolation and identification of SkMSCs. (A) Double-sorted SkMSCs were positively stained with antibodies against CD34 and integrin β1 and negatively stained for CD11b and CD45 in freshly sorted SkMSCs. (B) Immunofluorescence staining images for antibodies against Pax7 (red) and MyoD (green). Cell nuclei were stained by DAPI (blue). (C) After culturing in DMEM supplemented with 2% heat-inactivated horse serum, the cells showed more robust expression of MyoD over time, while PAX7 showed the opposite

expression pattern. GAPDH was used as an internal control. (D) Quantification of Pax7 and MyoD normalized to GAPDH. (E) Quantitation of Pax7-, MyoD-, desmin-, and MYHC-positive cells. Marker-positive cells are presented as the percentage of the total cell number using triplicate samples. Each bar represents the mean ± standard error of the mean (SEM). *P < 0.05, **P < 0.01, and NS = nonsignificant difference.

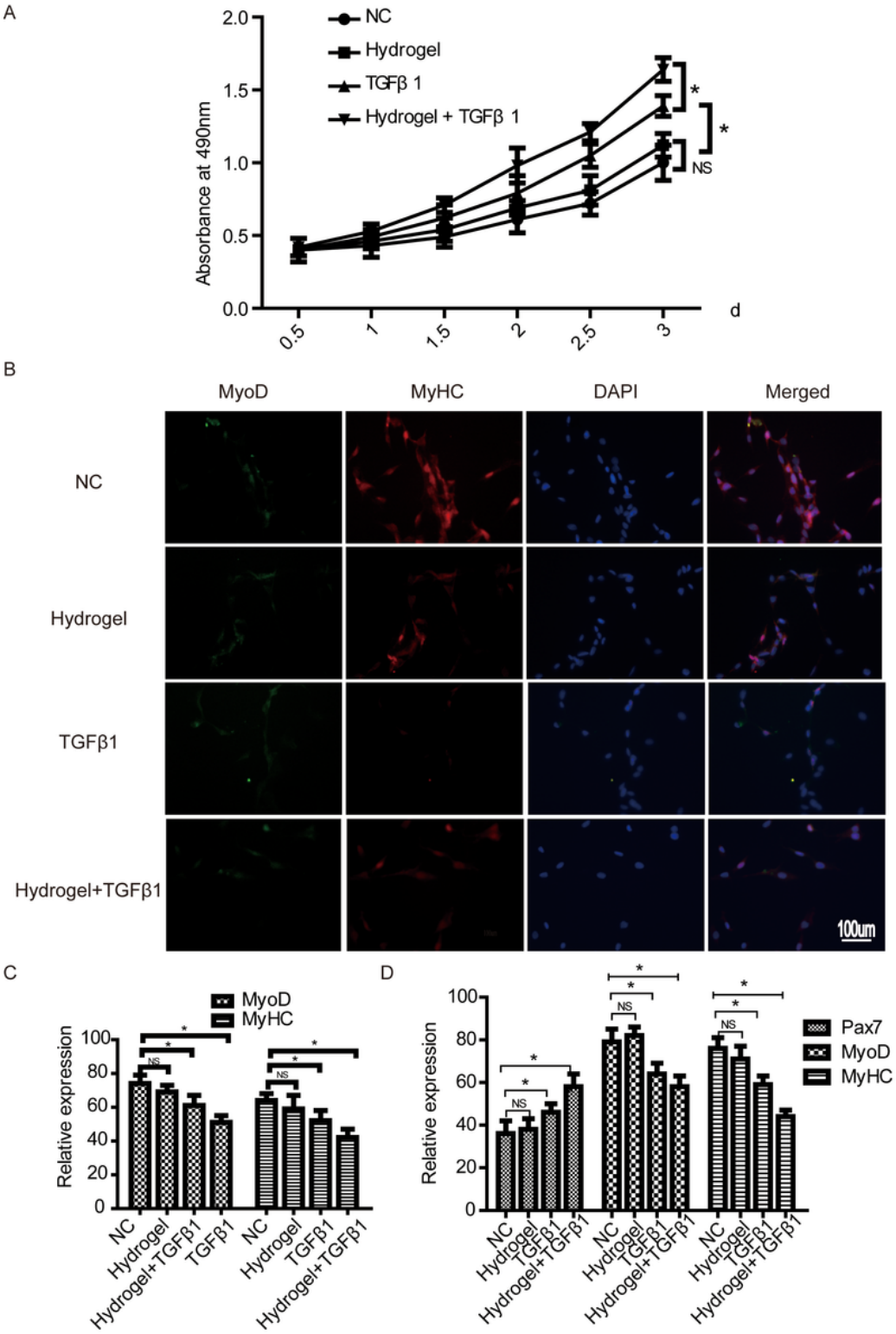

Figure 4

Effect of decellularized aligned skeletal muscle ECM hydrogels with TGFβ1 on the proliferation and differentiation of satellite cells. (A) Cell viability was analyzed by an MTT assay of the NC, hydrogel and hydrogel + TGFβ1 groups. (B) Immunofluorescence staining images of the expression of MyoD and MYHC in the three groups. (C). Quantification of MyoD and MYHC. (D). Pax7, MyoD and MYHC protein expression in the three groups was examined by western blot and quantified (E). Each bar represents the mean ± SEM. *P < 0.05.

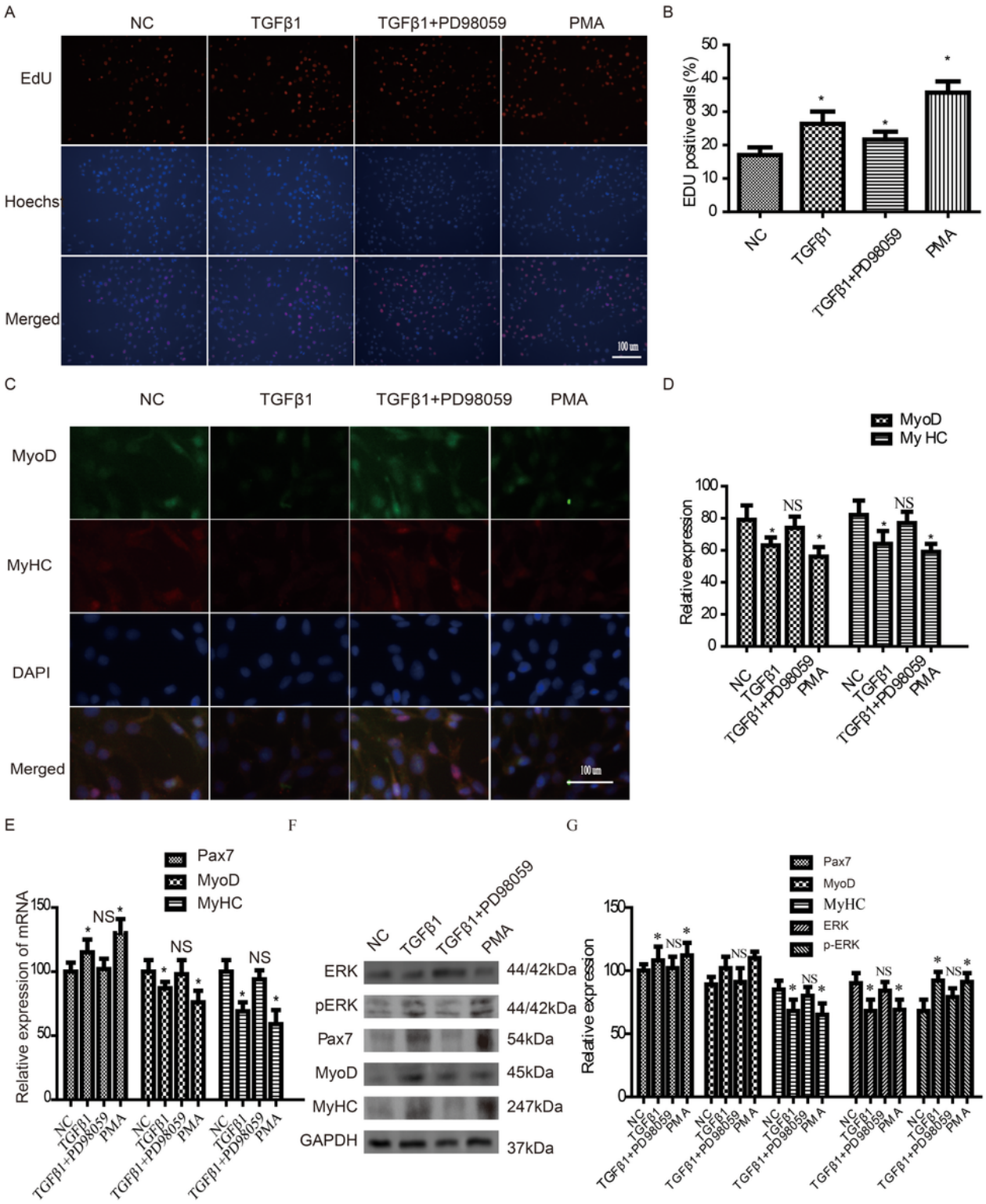

Figure 5

Decellularized aligned skeletal muscle ECM hydrogels with TGFβ1 analyzed for the proliferation and differentiation of satellite cells by ERK signaling. (A) EdU assays demonstrated the proliferation of SkMSCs in the different groups. (B) Quantification of Edu-positive cells in the different groups. (C) Immunofluorescence staining images of the expression of MyoD and MYHC in the four groups. (D) Quantification of MyoD and MyHC. (E) Relative expression of Pax7, MyoD and MyHC mRNA in the different groups analyzed by qRT-PCR. (F) Pax7, MyoD and MyHC protein expression in the different groups was examined by western blot and (G) quantified. Each bar represents the mean ± SEM. *P < 0.05, NS = nonsignificant difference.

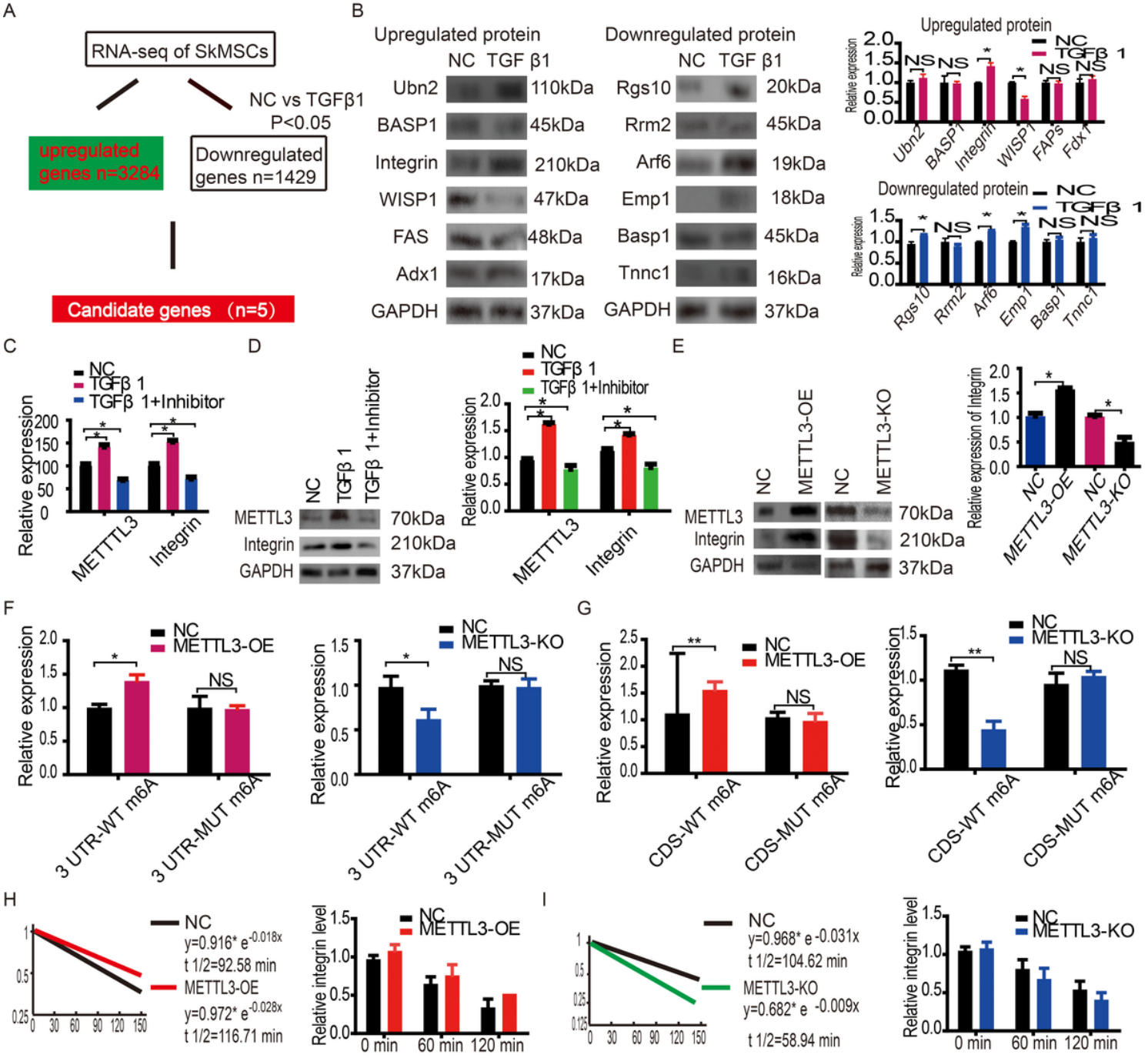

Figure 6

The expression of integrin in SkMSCs with TGFβ1. (A) Flowchart of the screening process of candidate genes. (B) western blot analysis demonstrated the five of most significantly upregulated and downregulated genes in SkMSCs in the different groups. (C) The expression of METTL3 and integrin was assessed by q-PCR. (D). METTL3 and integrin protein expression in the three groups was examined by western blot and quantified (E). Integrin protein expression due to METTL3 overexpression and METTL3-KO was examined by western blot and quantified. (F, G) Luciferase reporter and mutagenesis assays. Each stable cell line was cotransfected with integrin-CDS orintegrin-3'UTR bearing wild-type or mutant. (H, I) Effects of METTL3 on integrin mRNA stability. *P < 0.05, **P < 0.01. Each bar represents the mean ± SEM. *P < 0.05.

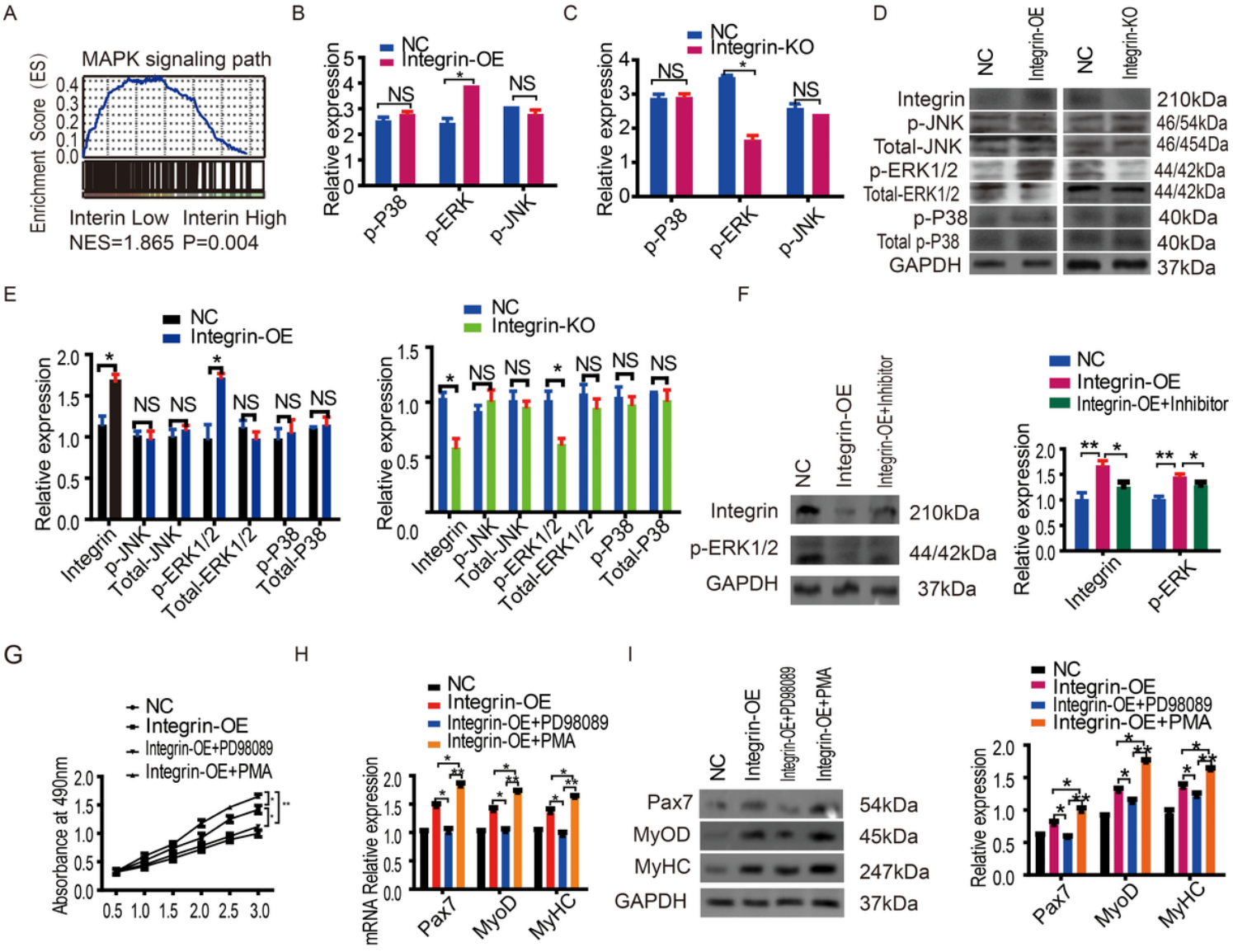

Figure 7

METTL3 regulated the proliferation and differentiation of SkMSCs through integrin-induced ERK signaling. (A) Gene set enrichment analysis (GSEA) identified a significant association between integrin and the MAPK signaling pathway. (B, C) phosphokinase microarray assay analysis of the SkMSCs. (C, D, E) Representative images of critical members of the MAPK signaling pathway was examined by western

blotting in SkMSCs. (F) The expression of integrin and p-ERK western blot in SkMSCs. (G) The effect of integrin downregulation on SkMSCs proliferation. (H, I) The effect of integrin on the expression of Pax7, MyoD and MyHC. *P < 0.05, NS = nonsignificant difference.